Development of a Novel Pixelated Time Projection Chamber Detector: Q-Pix

Dissertation by
Kevin Keefe

A DISSERTATION SUBMITTED TO THE GRADUATE DIVISION OF THE UNIVERSITY OF HAWAI‘I AT MĀNOA IN PARITAL FULFILLMENT OF THE REQUIREMENTS FOR THE DEGREE OF
DOCTOR OF PHILOSOPHY
IN
PHYSICS

KE KULANUI O HAWAI‘I MA MĀNOA
Mānoa, Hawai‘i

April 2023
Dissertation Committee:
Kurtis Nishimura

Chairpersons
Jason Kumar, John Learned, Scott Rowland, Peter Sadowski, Gary Varner
Keywords: Field Programmable Gate Array, Time Projection Chamber, Diffusion

Kevin Keefe
ORCID: 0000-0000

ACKNOWLEDGEMENTS

ABSTRACT

The Standard Model (SM) of physics has proven remarkably successful in past decades, yet some measurements such as neutrino oscillations show that this model is still an incomplete description of nature. The hunt for New Physics (NP) continues at higher energies ($>> 1GeV$) with larger detectors ($\approx 10kT$); the data acquired continually hint at Beyond Standard Model (BSM) physics. One such future detector is The Deep Underground Neutrino (DUNE) detector, which has recently begun construction. This 40-kT scale detector requires high precision in both timing ($<< \mu s$) and spatial resolutions ($\approx 1mm$) for vertex reconstruction of interesting neutrino events. DUNE (as any beam detector) is a combination of two detectors, a near-detector (ND) and a far-detector (FD) for long-baseline neutrino oscillation measurements. In order to meet the required timing and spatial resolution the DUNE-FD is a Liquid Argon Time Projection Chamber (LArTPC) design. Recent work has been done to show that LArTPCs can transition from a traditional wire readout to a pixelated readout, and thus further improve vertex reconstruction. This dissertation discusses recent progress and characterizations of a novel implementation of new a pixelated LArTPC readout technology. This novel readout is based on a charge-integrate-reset circuit at the pixel level (Q-Pix). We present the basic pixel-level readout circuit and the implications such an implementation has when applied at DUNE-FD scales. Further, we demonstrate results from the first-prototype implementation based on Q-Pix has been successfully used with solely over-the-counter electronics to acquire new Liquid Argon diffusion measurements. One crucial problem of any pixelated readout is the the ability to handle a large number of unique data channels ($\approx 100k$). To address the scaling problem we developed and tested a modular digital back-end prototype, and implemented it within the first LArTPC prototype. Next, we discuss nominal DUNE-FD APA system level requirements to achieve a projected required sensitivity, remove backgrounds, pixel-level calibration techniques, and possible methods for particle-identification (PID). Simulation results are also performed based on projected background and high-energy neutrino beam-line events. Finally, based on these results of the prototypes and simulation we discuss the nominal digital back-end readout constraints of a fully realized QPix implementation for a DUNE-FD Module.

TABLE OF CONTENTS

LIST OF ILLUSTRATIONS

LIST OF TABLES

Number *Page*

Chapter 1

INTRODUCTION

This chapter outlines and highlights useful background that will be explored in further detail in upcoming chapters as well as provides an outline for the thesis.

We begin with an overview of the standard model, and how both its success and short comings drive larger and more expensive detectors at the intensity frontier. To elucidate the issues at the forefront of the standard model we provide a brief history, with an emphasis on the detectors and experiments which helped lead to its formulation. Next, we become more specific and discuss DUNE which is an example of a new, large, and expensive detector which aims to push beyond the Standard Model. Finally, we finish this section on a discussion on the developments of new tracking detectors and their relevance to the work presented here.

1.1 The State of Things: The Standard Model

What is the universe made of? What are the fundamental building blocks of matter? Since time immemorial thinkers have questioned the nature of the universe and wondered what the basic building blocks of nature are. The answer to these fundamental questions is the motivation for particle physics.

In the history of science, it is easily argued that the most successful of all models has been the Standard Model of physics. The Standard Model (SM) [1–3] was originally developed in mid to late 1970's, and is the model responsible for unifying the weak, strong, and electromagnetic forces together. It has been made remarkable predictions about the existence of elusive neutrinos, quarks and vector bosons before their discovery, and more.

The comprehensive and extensive list of known particles as well as various cross-sections and lifetimes can be found from the bi-annually published Particle Data Group (PDG) [4]. The SM has been experimentally tested to limits unlike any other theory. It was gradually developed in the 1970's as a result of the boom of particle detectors in the middle and late 1960's.

In this section we briefly describe the SM and highlight some (certainly not all) key aspects of its formulation as understood today. The SM has stood the test of time, despite many known failures

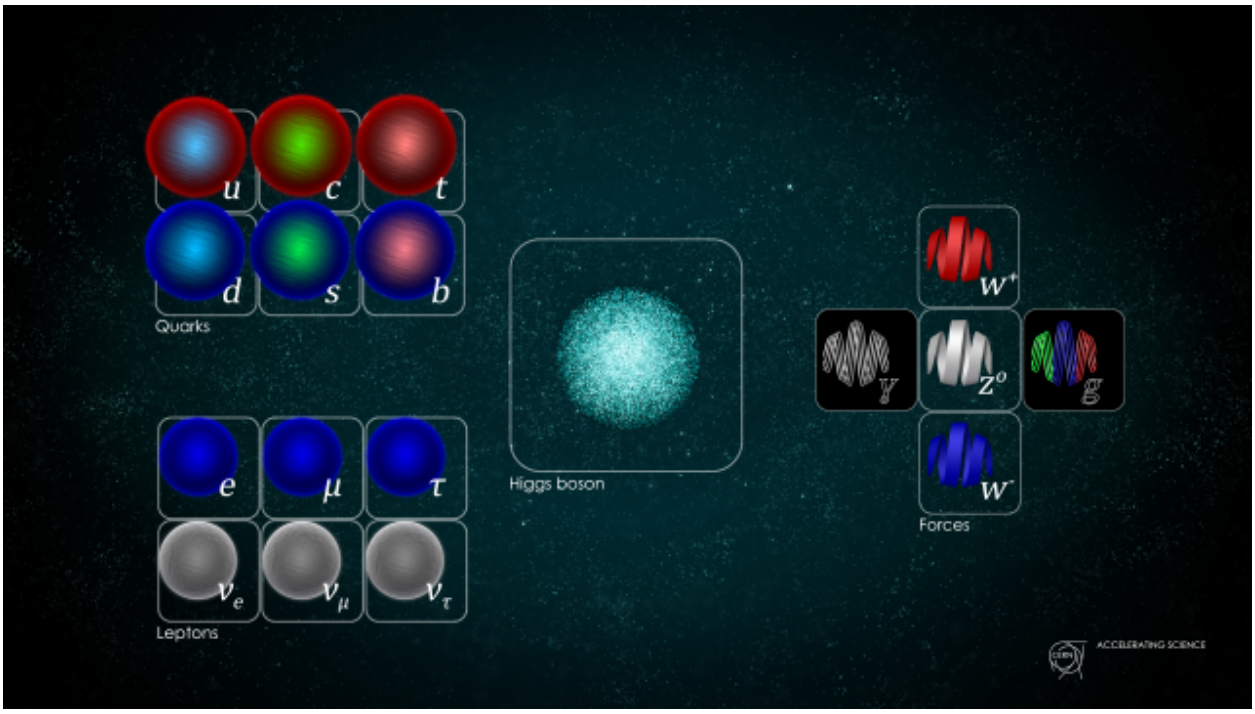

Figure 1.1: Image of Fundamental Particles in the Standard Model, taken from CERN website [5]. All known matter and particle interactions involves combinations of the particles listed here.

and holes in its predictions. Therefore, we hope to elaborate a bit on its status and predictions to help the reader better appreciate the significance of looking for physics beyond the SM.

The basics of the Standard Model

The SM itself dictates what the fundamental constituents of matter and energy are. As any theory in science its purpose is to explain observed phenomena. In this case, the observed phenomena is simply all particle interactions which involve mass or energy.

The interactions described by the standard model involve the fundamental particle interactions via three of the four known fundamental forces observed in nature: electromagnetic, weak, and strong forces. One of the current failings of the SM is its inability to incorporate a quantum description of gravity. The discussion of the re-normalization of quantum-gravity is beyond the scope of the work presented here, and so we only mention that it has to be achieved.

All known fundamental particles are represented in Fig. 1.1. These particles represent the current best knowledge of the building blocks of all observed matter in the universe.

Quarks

The quarks represent particles in the top left of Figure 1.1.

Quarks are the fundamental particles which constitute the "normal" heavy particles, such as protons and neutrons. Quarks also have unique anti-particles partners of each other. As do all anti-particles, the anti-quark counter-parts have the same mass as the normal partners with all quantum numbers interchanged.

A unique feature of Quarks compared to the leptons is that no "free" Quark has ever been observed. Most commonly, the quarks combine in pairs or in triplets to make mesons or baryons, respectively. Even more complicated constituents can be made of additional quarks, such as tetra and penta quarks, so long as all of the quantum numbers are unique for each quark.

The mesons contain a quark and an anti-quark, whereas the baryons a contain three quarks. Collectively, all particles constituted by any combination of quarks are known as hadrons. In 1961 Murray Gell-Mann proposed his "eight-fold way" [6] which provided a method of grouping the hadrons.

Since quarks are not freely observable a common place to infer their existence (and to create heavier hadrons) are in particle accelerators. The most well known particle accelerator is the Large Hadron Collider (LHC) in Geneva. These Particle accelerators generate extremely high energy ($\approx \mathcal{O}(10TeV)$) protons which when collided can generate new composite hadrons of any mass so that the total energy is conserved.

Since quarks, due to their color, readily combine to create more easily observed composit particles. The Quark model was then propossed by Gell-Mann in 1964 [7]. This model is a group theory concept (known as SU(3) symmetry) and is the means for which the fundamental particles (quarks) combine into the composite particles (hadrons) which are more readily and easily measured today. Eventually experiments conducted at the Stanford Linear Accelerator (SLAC) between 1967-1973 verified the existence of these quarks and Gell-Mann won the Nobel Prize in 1969.

The rescue of the quark model came with the measurement of [8]. The J/psi particle indicated the existence of a fourth since then unmeasured quark, which we now know as the charm (c).

Leptons

The leptons represent particles in the bottom left of Figure 1.1.

Quark	Charge	Mass (MeV)	Year Discovered	Ref.
up	$\frac{2}{3}$	2.16	1968	SLAC [9, 10]
down	$\frac{-1}{3}$	4.67	1968	SLAC [9, 10]
strange	$\frac{-1}{3}$	93.4	1968	SLAC [9, 10]
charm	$\frac{2}{3}$	1270	1974	SLAC [8]
bottom	$\frac{-1}{3}$	4180	1977	Fermilab [11]
top	$\frac{2}{3}$	173000	1995	Fermilab [12]

Table 1.1: Description of the discovery of quarks. Notice that as the mass increases for a particular quark the year of discovery also increases. This is a property of how we create and observe the quarks in our accelerators, and also the reason why physicists continue to want to build bigger ones. Interesting physics happens at higher and higher energies, which require larger and more expensive detectors to probe these energy scales. Note that the lighter quark masses are not well understood for other experimental reasons, and the presented data are rounded to three significant figures based on [4].

The first lepton discovered, and the most easily recognized, is the electron which was discovered by J . Just like the quarks, the leptons come in three families (electron, μ, τ). Also like the quarks, the leptons have charge, mass, and flavour which means they can decay.

Unlike the quarks the leptonic particles do not have a color quantum number and therefore do not combine together to create composite particles. Additionally, free leptons are observed, e.g. the electron.

The most difficult to measure fundamental particles of within the SM are the neutrinos. This is because these leptons carry no net charge. However, since they carry flavour and can decay (or be absorbed) and they also carry their respective lepton number, the neutrinos in the family can be identified by measuring their partner.

For example, a common process to observe an anti-electron neutrino ($\hat{\nu_e}$) is through inverse beta-decay (IBD) following the reaction:

$$\hat{\nu_e} + p \rightarrow e^+ + n \tag{1.1}$$

This IBD reaction is a common measurement tool for identifying neutrinos because of the distinguisable detection signature of the produced particles. The position (e^+) annailates very quickly ($\approx \mathcal{O}(ns)$) and will produce back-to-back 511 keV photons. The produced neutron, on the other hand, wobbles around much longer ($\mathcal{O}(us)$) before being captured, which produces scintillation light of energy proportional to the neutrons energy when captured.

Lepton	Charge	N_e	N_μ	N_τ
e^-	1	1	0	0
ν_e	0	1	0	0
μ	1	0	1	0
ν_μ	0	0	1	0
τ	1	0	0	1
ν_τ	0	0	0	1

Table 1.2: Description of the quantum numbers of the fundamental lepton families. There are three unique families within the leptons: electron, muon, and tau. The charge carrier as well as the neutrino each carry a value of one for this number. Their anti-particle counterparts carry -1 of this number.

The muon (μ) was discovered by Anderson and Neddermeyer in 1936 by observing cosmic ray showers [13].

The tau (τ) was discovered by SLAC in 1975 [14].

The first measurements of the neutrinos in each family were much harder than their charged partners. The electron neutrino (ν_e) and the muon neutrino (ν_μ) are observed in decay interactions.

The tau neutrino (ν_τ) was exceptionally difficult to measure. Like the previous neutrino partners, the ν_τ is discovered by looking for the creation of its partner (τ) during a CC interaction. As a comparison the τ has a lifetime of only 10^{-13} s whereas the muon life time $T_\mu \approx O(1\mu s)$ or seven orders of magnitude shorter!

The first successful experiment came in 2000 [15]. DONUT utilized a much more complicated emulsion detector to collect tracks from a 800 GeV proton beam offline. The exxperiment collected a total of 203 neutrino interactions, of which it found evidence for a total of only four interactions.

Forces

All forces within the standard model (electromagnetism, weak, and strong) are governed via a "carrier" particle. These carrier particles are represented on the center-right of 1.1.

The electromagnetic force is governed by particle exchanges of a photon. Other than perhaps gravity, which isn't explained by the SM, this is the most well known and described force. All particles which carry charge interact via this force. Therefore the neutrinos are the only particles

Force	Scale	Theory	Carrier	Ref.
Strong	10	Chromodynamics	gluon	TASSO [16]
Electromagnetic	10^{-2}	Electrodynamics	photon	Planck?
Weak	10^{-13}	Flavourdynamics	$W^{\pm}$,Z	CERN [18],[19]
Gravity	10^{-42}	General Relativity	graviton	??

Table 1.3: Relative strength chart of the four fundamental fources of nature. Although gravity is not included within the SM it is included, as well as its theoretical force carrier the graviton.

within the quarks and leptons which do not interact at all with the electromagnetic force (this is why detecting them is so hard). The full theoretical description of this force is governed by Quantum-Electrodynamics (QED).

The weak-nuclear force is governed by particles exchanges of one of the three particles in the center: $W^{\pm}$ and Z. This force involves a change in flavor of a particle, and involves both quarks and leptons. It is also responsible for all decay processes. The theoretical description of these mechanics are called Quantum-Flavourdynamics (QFD).

The strong-nuclear force is governed by the exchange of the gluon (g). This force is responsible for color changes of matter and describes why nuclei are held together. Since this force only involves exchanges of a gluon, the leptons are therefore unaffected since these particles carry no color quantum number. The full theoretical description for the strong-nuclear force is Quantum-Chromodynamics (QCD).

The gluon was discovered in at the TASSO experiment 1979 [16, 17].

Measurements of the intermediate bosons were much harder. The $W^{\pm}$ boson were measured in 1983 [18]. Followed by the Z boson which was measured shortly afterwards in the same experiment [19].

Higgs

The last particle to be discovered in the SM was the Higgs particle. The Higgs particle was originally predicted in 1964 by Peter Higgs [20]. This particle is important to describe how mass is given the the elementary particles described by the SM. Finally, in 2012 the Large Hadron Collider (LHC) was able to infer the massive Higgs particle [21].

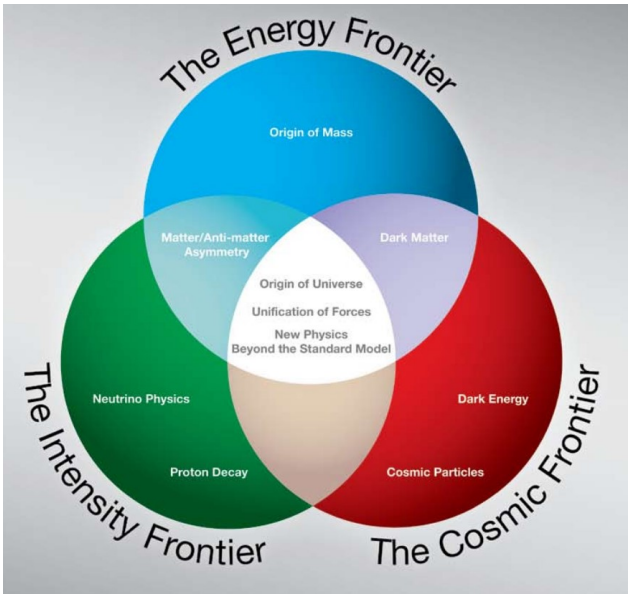

Figure 1.2: Image based on the 2008 P5 report [22]. The white text labeled within each frontier describes the search for some physics beyond the SM within that frontier.

The Frontiers of the Standard Model

Despite its (SM) numerous achievements in predictive power and experimental verification we know today that it has crucial shortcomings. The Standard Model (SM) [1–3] has no ability to account for Dark Matter or Dark Energy in the universe, nor the distribution (or the hierarchy) of neutrino masses, nor is it able to relate how gravity interacts with the other fundamental forces of nature (Unification). It also doesn't account for some 'basic' properties it has, such as: why are there only three generations of leptonic particles (electron, muon, and tau)? These short-comings offer hints for where to search for physics. Physicists have known about these short comings from the conception of the Standard Model and have (to no avail) sought out what's next.

With a plethora of hints to search for New Physics (NP), it can be useful to organize the efforts of search. In 2008 the Particle Physics Project Prioritization Panel (P5) did just this and labeled the three frontiers of physics: the cosmological, energy, and intensity frontiers. Each of these frontiers offer different kinds of challenges and serve as guides to look for physics beyond the SM.

Cosmological

The cosmological frontier aims to search for NP on extremely large time and distance scales by relying on observational techniques. Cosmological measurements have shown the that majority of

the universe's matter is not visible to light, and so we call it dark matter. Additionally, the universe is expanding at an accelerated rate, which we can tell from the blueshift of distance galaxies. Likewise, cosmologists have also discovered that the universe is expanding due to some invisible energy in the universe, and so we call it dark energy.

The search for these dark causes of the universe lie within the realm of the cosmological frontier.

Dark energy currently resides as the explanation for the observed accelerated expansion of the universe. Dark matter is commonly used to explain the deviation of the rotational frequency of galaxy clusters.

Energy

The energy frontier is concerned with the origin of mass. The Large-Hadron Collider (LHC) [21] experiment is the archetypal experiment aimed at solving problems within this frontier. The LHC itself consists of other large-scale tracking and calioremtry experiments such as ATLAS [23] and CMS [24].

Large particle accelerators are used to generator source particles of ever increasing energy. Due to the conservation of mass, the higher the energy of the particle accelerated the higher the mass (energy) of the particles created after certain collisions can be.

There also exist lepton collidors [25] which offer unique areas of search along this frontier too. More detailed descriptions of such collider experiments are beyond the scope of the work presented here, and further reading may be pursued from the extremely detailed technical design reports cited here of Belle-II and the ATLAS experiments.

Intensity

The third (and final) frontier we'll discuss is the Intensity frontier. The Intensity Frontier of Physics ([22]) is one which today requires very large and very precise measurements to gain the statistics to declare an observation. In order to address the issues posed within this frontier the large scale detectors hunting for New Physics (NP) have continued to grow in size, energy sensitivity, and importantly cost: [26].

As compared to the energy frontier which normally relies on creating new particles from accelerators the Intensity Frontier often searches for rare events, like a proton decay.

Neutrino searches also lie within this frontier. Neutrinos are notoriously difficult to detect and measure since they can only be probed via the weak-nuclear force, and even then only indirectly since they carry no charge themselves.

1.2 How we got here.

Many times since the early 20th century it was thought that the goal of physics was accomplished. However, during each of these moments of false triumph some new detector was built to take a new measurement; thus, the door to new understanding of nature is never closed. This section provides a brief and (necessarily) incomplete history of significant measurements and detector developments relevant to particle physics in the creation of the SM. In order to clear an obstacle, it is often helpful to remember the previous ones.

A Century of New Physics

At the turn of the 20th century particle physics was in its infancy. In 1900 Max Planck first introduces the concept of energy quanta for the first time concerning photons to eliminate the infamous ultra-violet catastrophe problem introduced by statistical mechanics. JJ Thomson used a single cathode-ray tube to discover the electron and the nucleus, and won for himself the Nobel Pize in 1906. Milikan's famous oil-drop experiment won him the Nobel Prize in 1923.

However, as each of these new discoveries solved problems only more questions were produced. Once the nucleus was discovered to contain only protons and neutrons, the natural question arose: what holds all of the positive charge together in the center. Thus, physicists cleverly named the new force which was stronger than the electromagnetic force: the Strong Force.

The bubble chamber was then invented in 1952 by Donald Glaser [27]. These detectors proved significant in the discover of the W and Z bosons and ultimately allowed the unification of the electromagnetic and weak forces to form the electroweak theory.

Next the spark chamber eventually lead to the gradual development of the wire-spark chamber. In 1968 Georges Charpak developed the Multi-Wire Proportional Chamber (MWPC) for which he (much later) won the Nobel Prize in 1992. From this key insight a new detector concept was made possible.

Modern Tracking Detectors

It is could said that any definition defining a "new" age of a types of detectors is subjective. Nevertheless, we proceed to define that modern particle detectors were the age that began to use

modern electronics, or electronics after the development of the metal–oxide–semiconductor field-effect transistor (MOS-FET). If there was any invention which was able to drive the development of computers and measuring electronics, it was the transistor. Therefore, the beginning of the modern particle detection age began with the transistor, and it saw to the end of the spark chamber and bubble chamber detectors.

Multi-Wire Proportional Chamber

The middle of the 20th century saw a dramatic increase in the ability and reduction of the cost of electronics. These (then) new electronics allowed for fast digitizing measurements of voltage or current. Thus, new propotional counter detectors were capable of using computers to do the measuring or counting of the events within the detector. The rate at particles could then be detected increased by orders of magnitude.

Using the fast digitizers and closely spaced wires Georges Charpak (1924-2010) created the first-Wire MWPC in 1968 [28]. This new detector was one which paved the way for modern detector development, for which Charpak won the 1992 Nobel Prize.

Time Projection Chambers

Time Projection Chambers (TPC) [29] have been shown to be extremely useful in high energy physics experiments due, in part, to their high resolution in both timing and spatial dimensions. This detector was originally used in the Position-Electron Project PEP-4 experiment which measured electron-positron collisions from the 29 GeV electron beam produced at the Stanford Linear Accelerator (SLAC). The first TPC design used high pressure gas and was able to measure 1000s of particle tracks per second (compared to 1-10) and provide full 3-D event reconstruction.

It did not take long for other experimentalists to generalize this concept to different elements or even to liquid.

Noble Gases and Time Projection Chambers

The technology of TPCs has greatly matured since their original inception. in many kinds of detectors across HEP. TPCs can also incorporate two phases of a substance (liquid and gas), called Dual Phase (DP) TPCs.

the Xenon-1T is a dark matter experiment which is a dual-phase TPC [30].

The LUX experiment is a single phase TPC also hunting for dark matter.

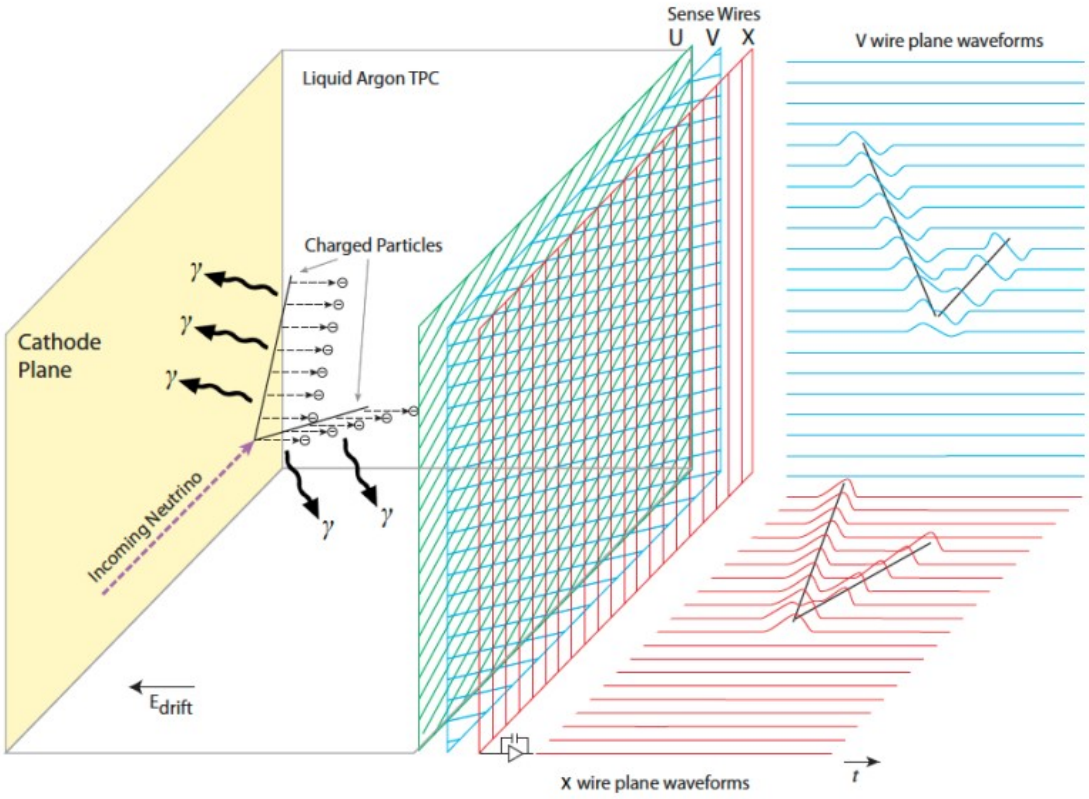

Figure 1.3: Image of a Time Projection Chamber (TPC). Charge is accumlated within the volume as ions are removed from the fidicial volume from another charged ion as it passes through the material. An uniform electric field drifts the free now electrons towards the anode plane. The collection and readout of charge on this anode plane is what is recorded within the detector. Image is taken from [31].

A specific kind of TCP is a Liquid Argon Time Projection Chamber (LArTPC) [32].

Recent work on LArTPCs ([33–35].)

Energy resolution of the LArTPCs within DUNE are still unknown to within a factor of 4 [36].

1.3 Ways Forward

Despite the passing of generations of detectors and developments in electronics the SM remains. For nearly 50 years now the SM is still our best model at describing nature as we know it, despite also knowing that there must be more. Here in this section we describe in some more detail current searches at the intensity frontier where physicists are looking to go beyond the SM.

We give special attention to neutrino oscillation at the end of this section since later chapters

simulation studies will be based off results hoping to measure this effect.

Hadron Decay

Does a proton decay? This is the fundamental question for physicists looking at hadron decay. The SM predicts that the proton itself is stable, thus it should never decay. However, physicists know that the SM is itself not a complete theory since, among other reasons, it does not incporate gravity. Attempts to unify all of the fundamental forces of nature into one unified theory are considered Grand-Unified Theories (GUTs), and according to many GUTs the proton does, in fact, decay.

Current measurements on the proton lifetime indicate that its lifetime is on the order of magnitude (or above) 10^{34} years. Even at its most frequent, this is an exceedingly rare event considering that the lifetime of the universe is $\approx O(10^{10} yrs)$

Since these events are so rare, extremely large detectors with large numbers of protons inside of them are required to constantly observe many protons. An example of a second generation proton decay studies is the Imaging Cosmic and Rare Underground Signals(ICARUS) experiment [37].

There are at least two prominant decay chains that are expected to be dominant, depending on the Grand-Unification-Theory (GUT) that hopes to go beyond the SM. The first one is:

$$p^+ \rightarrow e^+ + \pi^0 + 2\gamma \tag{1.2}$$

This interaction is easily detectable in cherenkov based detectors due to the emission of both the gammas as well as the high energy of the emitted positron. In fact, the worlds best estimate for proton lifetime comes from this decay-chain [38].

Other Supersymmetric GUT models predict instead [39]:

$$p^+ \rightarrow K^+ + \nu \tag{1.3}$$

In this case the Kaon is generally moving too slow to be measurable by cherenkov detectors. However, a TPC style detectors are still sensitive to its signature charge deposition. This is an interesting reaction since the worlds best limits are currently provided by the Super-Kamiokande experiment, which is itself a cherenkov based detector in water.

These searches are interesting, if albeit difficult, both due to the rareness of such an event. If any detector was able to clearly measure even a single proton decay, that would provide direct evidence for physics beyond the SM. Future detectors that will continue to probe for nucleon decay are DUNE, Hyper-Kamiokande, and JUNO [26, 31, 40].

Supernova Studies

A supernova occurs when a massive star runs out of the necessary elemental fuel for fusion at its core. When this happens the inward pull of gravity due to the mass of the star overcomes the reduced outward pressure from the nuclear fusion.

It has been nearly 30 years since the last observed neutrinos from a galactic core collapse supernova, SN 1987A [41]. Sensitivity to supernova neutrinos is crucial for understanding the mechanisms that govern particles at these extreme densities and pressures. Interestingly, because neutrinos are so weakly interacting, it is possible to observe their signature and arrival before the photons arrival of a Type-II supernova.

The principal interaction chain observable in a TPC is:

$$\nu_e + {}^{40}Ar \rightarrow e^- + {}^{40}Kr^+ \tag{1.4}$$

A LArTPC is sensitive to ν_e by measuring the signture of both the e^- and ${}^{40}Kr^+$.

More on Neutrinos

Another possible route beyond the standard model are detailed studies of neutrinos.

Hints at the existence of neutrinos began early last century. More than 100 years ago Chadwick was able to show that the energy spectrum from a decaying electron was continuous [42]. This unknown cause of the spectrum even lead some physicists to belief that perhaps the conservation of energy was violated. Wolfgang Pauli instead predicted a particle which he originally called the neutron to also be a decay product, but not easily observable. This third particle in the decay would explain the energy spectrum of the electron. Quickly however the particle name neutron was taken by a different neutral particle in 1932 [43] The discovery of the neutron and the continuous spectrum of beta decay forced Pauli to come up with a new theory attempting to describe beta decay [44].

Originally physicists held little hope that such an elusive particle would ever be detected. However, the motivation to save this conservation law lead Wolfgang Pauli to the first prediction (1930) of the

neutrino; the reason that the energy was a spectrum from the electron was that some of the energy was "taken up" by the neutrino. Finally, some 26 years later in 1956 was the first observation of the electron neutrino [45].

The discovery of the electron neutrino ν_e was the first of the three families to be discovered. A few years later the first reactor neutrino (ν_μ) was observed at Brookhaven National Laboratory (BNL) [46].

The first measurement of the τ neutrino (ν_τ) happened much later in 2001 [15]. this detector used nuclear emulsions.

Daya Bay [47] has also established measurements of electron anti-neutrino ($\bar{\nu_e}$) disappearance.

After this first discovery is when the the answers, followed by more questions, came. Since then, many large-scale experiments have been dedicated to measuring the three generations of neutrinos. [47–54]

All reliable information we have about neutrinos come from these large scale detectors.

Originally the mass of the neutrino predicted by the SM was massless. That was until the Solar-neutrino anomaly measured significantly less neutrinos than predicted [55]. The solution for this was oscillation.

Neutrino Oscillation

Here we provide a very general description of a model to describing neutrino oscillation. We elucidate the measureable parameters which govern this oscillation and describe how these values are currently measured in experiments today.

Of all known particles the most elusive (hardest to detect and measure) is the neutrino. For this reason the least is known about the neutrino. What we do know about the neutrino is there are three flavors each associated with their leptonic partners: the electron, muon, and tau.

Tokai to Kamioka (T2k) [56] has well established neutrino oscillation measurements.

It came as a welcome shock that neutrino oscillation was first measured. This oscillation indicates that a neutrino as it moves through space can change its state; a electron neutrino can oscillate into a muon neutrino or even a tau neutrino. This happens because the mass eigenstate and flavor eigenstates which govern the neutrino are not equal.

The standard notation which relates the mass eigenstates (ν_i) and flavor eigenstates (ν_α) ,

$$\nu_i = U_{i\alpha}\nu_\alpha \tag{1.5}$$

$$\begin{pmatrix}\nu_e\\ \nu_\mu\\ \nu_\tau\end{pmatrix} = \begin{pmatrix}U_{e1}, U_{e2}, U_{e3}\\ U_{u1}, U_{u2}, U_{u3}\\ U_{\tau 1}, U_{\tau 2}, U_{\tau 3}\end{pmatrix}\begin{pmatrix}\nu_1\\ \nu_2\\ \nu_3\end{pmatrix} \tag{1.6}$$

The matrix elements within U_{li} represent the mixing coeffecients and are used to calculate the prabability that a certain neutrino will oscillate from one family to another. We identify U_{ij} as the commonly known U_{PMNS} matrix, where PMNS stands for: Pontecorvo–Maki–Nakagawa–Sakata, or the four theorists who helped developed this convention. Luckily, there are not a total of nine free parameters within the SM that determine this. The U_{PMNS} matrix can be additionally rewritten following [57, 58] as:

$$U_{PMNS} = U_{sol} \times U_{rea} \times U_{atm} \times U_{maj} \tag{1.7}$$

After expanding the matrix representations, equation 1.3 becomes:

$$U_{PMNS} = \begin{pmatrix}1 & 0 & 0\\ 0 & C_{23} & S_{23}\\ 0 & -S_{23} & C_{23}\end{pmatrix} \times \begin{pmatrix}C_{13} & 0 & S_{13}e^{-1\delta_{cp}}\\ 0 & 1 & 0\\ -S_{13}e^{-1\delta_{cp}} & 0 & C_{13}\end{pmatrix} \times \begin{pmatrix}C_{12} & S_{12} & 0\\ -S_{12} & C_{12} & 0\\ 0 & 0 & 1\end{pmatrix} \times \begin{pmatrix}e^{i\alpha_1} & 0 & 0\\ 0 & e^{i\alpha_2} & 0\\ 0 & 0 & 1\end{pmatrix} \tag{1.8}$$

We identify above the additional matrix components where historically these values are measured. Therefore, instead of nine unknown parameters for the SM, there are only six. The components C_{ij} and S_{ij} in the matrices are defined to be $\cos(\theta_{ij})$ and $\sin(\theta_{ij})$, respectively.

Then, the six parameters of the U_{PMNS} are identified as:

- θ_{13}, reactor measurements.
- θ_{12}, atmospheric measurements.
- θ_{23}, solar measurements.

- δ_{CP}, Charge-conjugation parity violation.
- α_i, The two Majorana Phase parameters.

The Majorana phases (α_i) are sensitive in experiments that can detect the Majorana nature of neutrions such as neutrinoless double beta decay. In neutrino oscillation measurements, these phases cancel out and not not measureable. Therefore, we ignore these two phases for the remainder of this work.

Next we demonstrate the calculation of the probability of oscillation from one mass eigenstate to another. Namely we calculate the probablity $P(\mu \rightarrow e)$ which is the probability of interest in a long beamline experiment. First we identify that equation 1.3 can be rewritten to isolate the flavor-eigenstate terms (v_α) by multiplying by the adjoint of the PMNS matrix (U^*_{PMNS}). Then the relationship between the mass and flavor eigenstates become:

$$v_\alpha = U^*_{PMNS} v_i \tag{1.9}$$

The value of interest is $P(\mu \rightarrow e)$. The probability to end up in state v_e beginning from v_μ is:

$$P(\mu \rightarrow e) = |\langle v_e | v_\mu \rangle|^2 \tag{1.10}$$

We then use equation 1.3 to represent the matrix elements of U_{PMNS} from v_e and v_μ to obtain:

$$P(\mu \rightarrow e) = |\sum_i U_{ei} U^*_{\mu i} e^{-iE_i t}|^2 = \sum_i |U_{ei} U^*_{\mu i}|^2 + 2\Re(\sum_{i>j} U^*_{ej} U_{\mu j} U_{ei} U^*_{\mu i} e^{-i\Delta_{ij} t}) \tag{1.11}$$

Where we identify that the cross terms introduce a phase difference shown as Δ_{ij} in the second term in equation 1.3. This represents the neutrino oscillation term and represents the difference in the mass states of the neutrinos:

$$\Delta_{ij} = (E_i - E_j) \tag{1.12}$$

The energy of the neutrino in each state can be approximated to first order following:

Paramater	Best Fit	Unit
θ_{13}	$8.57^{+0.12}_{-0.12}$	na
θ_{12}	$33.44^{+0.77}_{-0.74}$	na
θ_{23}	$49.2^{+0.9}_{-1.2}$	na
δ_{cp}	197^{+27}_{-24}	na
Δm^2_{21}	$7.42^{0.21}_{-0.20}$	$10^{-5} eV^2$
Δm^2_{3l}	$2.517^{+0.026}_{-0.028}$	$10^{-3} eV^2$

Table 1.4: Known Oscillation Parameters of Interest. Values are taken from the global fit [62]. The values shown assume normal mass ordering for neutrinos and include atmospheric Super-Kamikonde Data.

$$E_i = \sqrt{p^2 + m_i^2} \approx p + \frac{m_i^2}{2p} \tag{1.13}$$

The momentumum of all of the mass eigenstates is the constant. Then oscillation parameter becomes:

$$\Delta_{ij} \approx \frac{1}{2p}(m_i^2 - m_j^2) = \frac{\Delta m_{ij}^2}{2p} \tag{1.14}$$

Finally, the last two parameters which govern the neutrino oscillations are identified as the mass differences between the three mass states. Now, the frequency of the oscillation between neutrino states depends on the difference of the square their masses (Δm_{ij}^2), where three neutrino masses imply two independent differences. The mass differences provide two additional parameters are needed to fully describe neutrino mixing. The six values of interest and their current best known fits are shown in Table 1.3:

The the sign of m_{13} is unknown. This leads to two possible ordernigs of the masses, known as normal and inverted, NO and IO respectively. The normal ordering indicates that the masses of the neutrinos follow the ordering of their charged partners. That is, NO implies a mass ordering of: $\nu_e < \nu_\mu < \nu_\tau$. Whereas, the IO has a mass ordering: $\nu_\tau < \nu_e < \nu_\mu$.

Neutrino oscillations in matter are slightly different than those in vacuum [60]. The Mikheyev-Smirnov-Wolfenstein (MSW) effect [61].

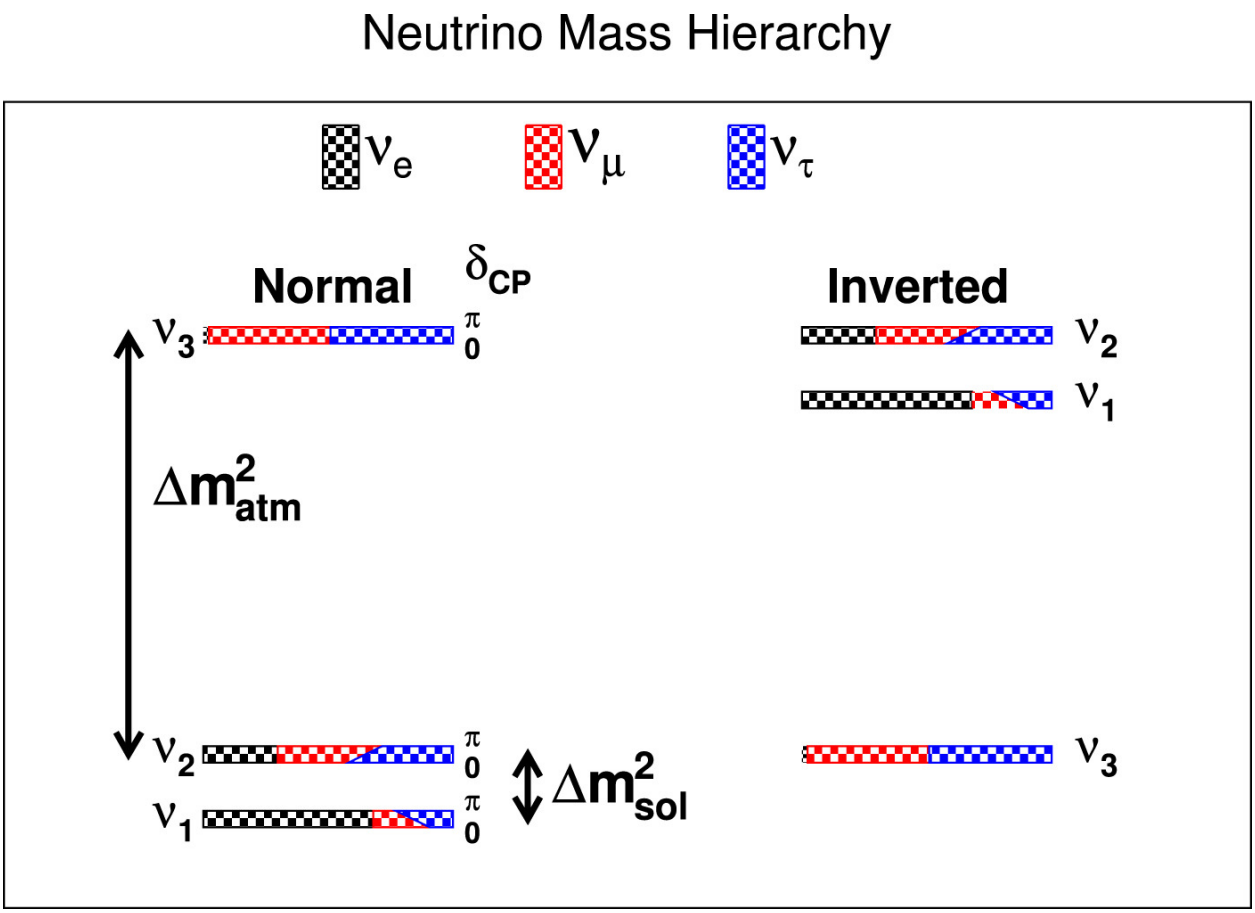

Figure 1.4: Representation of the mass hierarchy scales. This is a represntation of the two possible orderings of neutrino massses, due to the uncertain sign of m_{13}. It is also interesting to observe that the absolute mass scale is not measured since oscillation measurements only give difference mass squares. Image was taken from [59].

1.4 Detectors in the Current Century

Finally, in this last section we discuss the development of various upcoming detector technologies. There are many motivating pressures for new detectors to adopt pixelated designs. Below we discuss two contributing factors: the development of electronics and computing algorithms.

First, previously pixelated detectors have historically been more difficult because of the issues of cost and size regarding the number of readout channels. This is being addressed, in part, by the advent of newer, cheaper, and larger Field-Programmable-Gate Arrays (FPGAs). One method for reducing the electronic overhead required in pixelated detectors is to use digital multiplexing. Cheap, high channel FPGAs directly solve this problem. Other electronics development, such as the Silicon-Photomultiplier, offer much cheaper alternatives for large pixel counters compared to

their historical counter-parts.

[63] Another driving factor is the the development of Machine Learning (ML) algorithms, particularly Convectional Neural Network (CNN [64]). Recent industry has driven the need for CNNs to be able to correctly identify and label 2-D images of various kinds, and thus championed much of progress in this field and spawned many kinds of CNN algorithms. Recently, it has been shown how these kinds of algorithms extend into High Energy Physics (HEP) for particle identification. A major issue at the Intensity Frontier of physics is the sheer amount of data to store and process. These ML algorithms provied a developed tool to automate the analysis of huge amounts of data ($>> 1TB$) and have been shown to be quite accurate ($> 99\%$) at particle identification in LArTPCs.

Current Pixelization Efforts in TPCs

Additional work has been performed in recent years which show that LArTPCs can also utilized a pixel-based readout [65], [66].

SANDD

Another Example of a pixelated detector is [67].

The Single Volume Scatter Camera

This work is presented in greater detail in (Appendices-A/B) and represents a substantial amount of my own individual contribution. I am the 2nd author on the the paper described in Appendix-A and the corresponding author of Appendix-B, where I also collected and analyzed all presented data therein.

Future Detectors

The end of the Standard Model era is inevitable. SM simply fails to account for physics with all major frontiers for physicists to accept its completeness; we know there is much and more to learn about nature.

The 20th century saw unprecedented progress in its sophistication of its detectors from ray tubes, to spark chambers, to proportional counters, and to huge (>20 km) particle accelerators. This century shows no signs holding any less promise than its predecessor. Continued development in electronics, computing, and analysis methods will lead to more and newer frontiers of physics.

The work presented in this introduction aims to not only encapsulate the massive progress particle physics has made since the electron's discovery, but also to server as a reminder of how extraordinarily surprising nature is. At every turn and at every point where physicists think they've arrived at

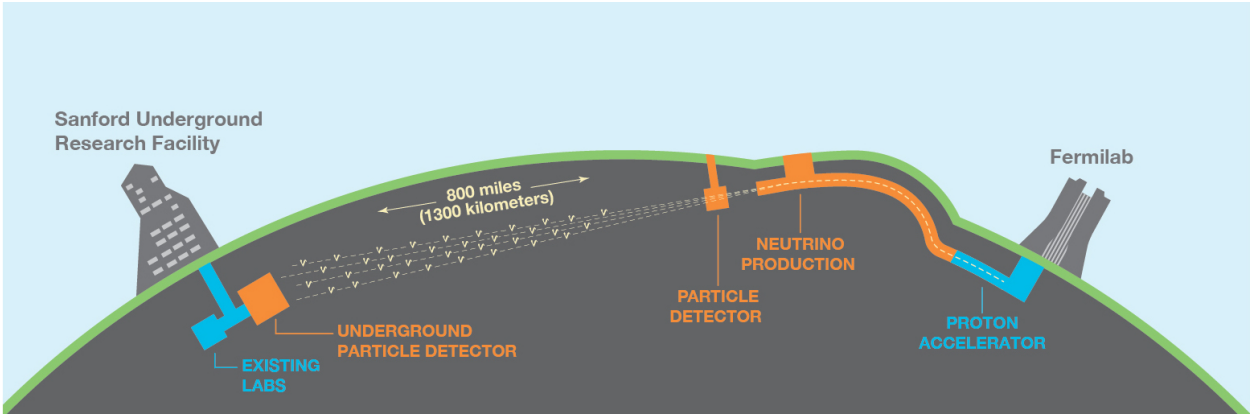

Figure 1.5: Representation of the Near and Far Detectors for the DUNE experiment. The Near Detector is located within the image labeled as the Particle Detector. One of the key purposes for the Near Detector is to tag outgoing particles from the proton beam. Image was taken from [71].

the end (or at an impossible roadblock) there always remains more to discover. If we have learned anything, we have learned to knock and the door shall be opened.

The Deep Underground Neutrino Experiment

The Deep Underground Neutrino Experiment (DUNE) is a long-baseline neutrino beam experiment [31, 68–70]. DUNE is composed two detectors, a near detector (ND) and a far detector (FD) which are separated by a distance of 1300 km.

The ND is located at Fermilab and its purpose is to characterize the source neutrino beam created there. The ND serves many purposes. To name a few

The FD will be placed underground at Sanford Underground Research Facility (SURF) and be approximately 1300 km away from the ND. This detector represents an enormous engineering challenge to place such large, cold, and complicated detector. The FD will be composed of up to four separate 10 kiloton modules.

The physics program

Two of these four modules at least will use a known wire-based readout technology and a vertical drift-readout. The two remaining modules are considered modules of opportunity and their readout technology is yet unknown. A purpose of this dissertation is show the viability of a novel readout technology.

DUNE has three main science goals, all of which are geared towards pushing beyond the standard

model:

- Hadron Decay
- Core-collapse Supernovae
- Neutrino Oscillation.

We will discuss the relevance of each of these items, and in 2 we will further discuss how the work presented here relates to each of these topics.

DUNE plans to offer an incredibly rich searches across the sectors listed above 1.4. We briefly discuss the relevance of some the searches below, but more detailed reading can be pursued at [68].

Conventional horizontal drift detection for foreseeable DUNE modules are already considered possible for lengths up to 6.5m [72].

Chapter 2

A NOVEL READOUT TECHNIQUE FOR TPCS: Q-PIX

In this chapter we introduce a novel pixel-based readout technology for TPCs. Pixel based readouts offer several advantages over the traditional wire readout [73]. A key improvement offered is true 3-D image reconstruction. This allows for sharper vertex reconstruction, thereby improving the overall resolution of DUNE and decreasing the required time for a NP measurement. Other advantages are ease of data analysis and reduction in total data storage. A pixel based readout automatically records two of the three spatial dimensions, and thereby provides for simpler analysis. Additionally, the pixelated readout method presented here cuts the total required data storage and data acquisition rate (without loss to precision) by several orders of magnitude.

However, the advantages also come with the cost of increased design complexity as the number of readout channels increases by more than three orders of magnitude. The traditional wire based readout within a DUNE module will include hundreds to thousands of channels, whereas a full DUNE module with a pixel-based readout will have 10's of millions of channels. This number of required channels to be stably readout during DUNE's expected lifetime (> 10 years), where the electronics continually operate at liquid argon temperatures is likely the largest hurtle for a pixel-based design. The aim of this dissertation is to address the channel-size problem.

2.1 Q-Pix: The Circuit Level Design

The fundamental readout circuit (2.1) was first introduced by Nygren and Mei [74]. The principle of the front-end circuit operates on measuring the output of a schmitt trigger whose comparator voltage input is connected to an integrating capacitor circuit.

The circuit input is connected to the anode of a TPC where drifted electron charge accumulates. Voltage is then built up from the charge stored on the pixel based on the capacitance according to the equation:

$$Q_i = C_i V_i \tag{2.1}$$

After the capacitor voltage (V_i) exceeds a set threshold value the schmitt trigger activates. The time

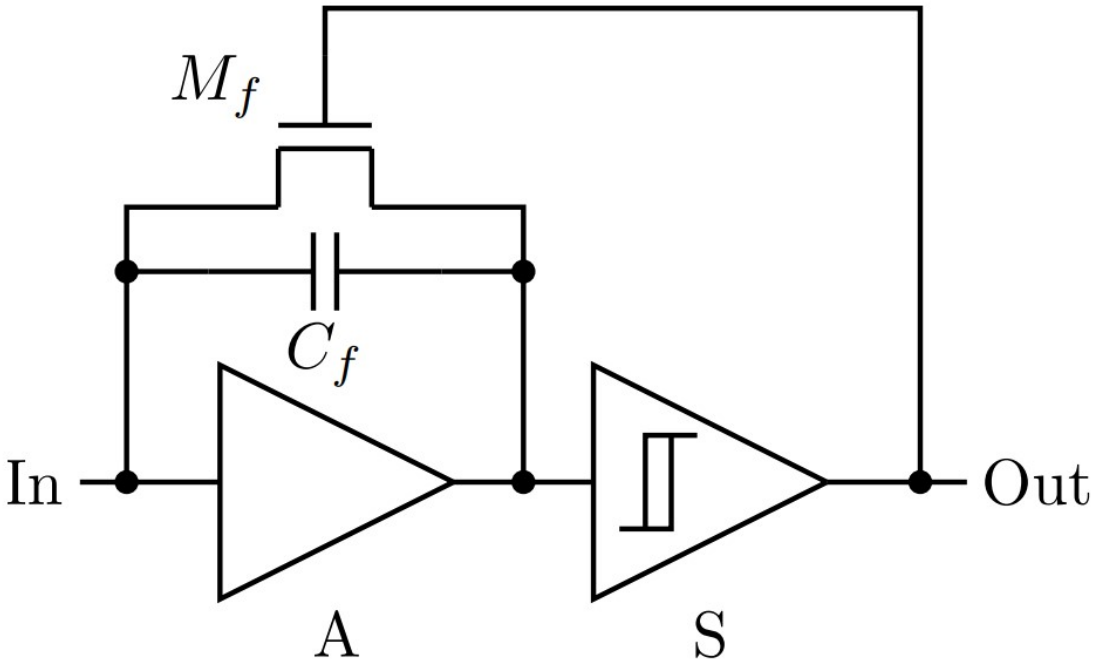

Figure 2.1: Image of Basic Q-Pix Readout circuit. Currently this front-end circuit is being designed as custom analog ASIC which has 16 channels. Image is taken from [74].

of the trigger output is recorded by a digital logic which encodes this data as a 32 bit value. Since the capacitor reset happens at the same time as the issued trigger the digitally-recorded value is the reset time.

We consider that the digital blocks responsible for digitizing the reset to have a nominal frequency of $\approx 30MHz$. Therefore, the minimum time before the recorded time value on each digital clock is calculated by

$$T_{loop} = \frac{2^{32}}{30 * 10^6} \approx 143 seconds \tag{2.2}$$

This time (T_{loop}) indicates the minimum reset time to occur within each responsible digital block.g; Since this time is much greater than the antipcated reset rates to be produced from backgrounds, discussed in a later section 2.1, we expect the looping of the 32-bit recorded value to not be a problem.

Reconstructing Voltage from Time Resets

Here we describe the basic principle of reconstructing the input current from a collection of reset measurements. The key insight for this readout technology is that time (instead of voltage as in a MWPC) is recorded. Therefore, measurements only taken place when there is enough charge to cause a reset which prevents continuous measurements during periods of long dead time. This concept follows the detector concept of least action in that all measurements are detector responses.

A measurement of a reset indicates that a certain amount of charge was discharged from the integrating capacitor. Since total charge is conserved, we can say that the total amount of charge that accumulates onto the pixel is equal to total amount of charge discharged from each reset, plus any residual charge still on the pixel. Therefore, we can relate the total accumulated charge to the total charge discharged with the following equation:

$$Q_{in}(t) = Q_{out}(t) + Q_c(t) \tag{2.3}$$

eq:qin)

If we assume that each reset removes the same amount of charge during each reset then we can rewrite Q_{out} in terms of N_t where N_t is the integer number of resets at time t:

$$Q_{out}(t) = Q_o * N(t) \tag{2.4}$$

eq:qout)

Where Q_o is the fixed amount of charge discharged during each reset. Equation **??** then can give us the maximum current output using the definition of current $I = \frac{dQ}{dt}$, then

$$I_{max} = \frac{d}{dt}(Q_o * N(t)) = Q_o \frac{dN}{dt} = Q_o * f \tag{2.5}$$

eq:imax)

Where we identify that the maximum value of $\frac{dN}{dt} = f$, with f as the clock frequency of the local digital block. Equation **??** relates the maximum current to the digital clock frequency and the amount of charge discharged during each reset. Then we take the nominal expected frequency , charge, and voltage values to calculate an expected I_{max}:

$$I_{max} \approx 1\ fF * 1\ V * 30 * 10^6 MHz \approx 30\ nA \tag{2.6}$$

We note that 30 nA is much greater than the expected background current from Ar^{39} ($\mathcal{O}(10^{-18})A$). However, the more interesting events deposit more more charge, and we can use the average drift speed of electrons in a LArTPC to estimate the maximum charge density we can be sensitive to:

$$\lambda_{max} = \frac{dQ}{dL} = \frac{dQ}{dt} / \frac{dx}{dt} = \frac{I_{max}}{v_{drift}} \tag{2.7}$$

We use a nominal v_{drift} speed of 1.6mm / μs, and convert to SI units to obtain λ_{max} in equation 2.1:

$$\lambda_{max} = \frac{3 * 10^{-8} A}{1600 \frac{m}{s}} = 1.875 * 10^{-11} \frac{C}{m} \approx 19 \frac{nC}{mm} \tag{2.8}$$

We can now use this result to calculate a maximum $\frac{dE}{dx}$ measurement:

$$\frac{dE}{dx}_{max} = \frac{dQ}{dx}_{max} \frac{dE}{dQ} = \lambda_{max} \frac{dE}{dQ} \tag{2.9}$$

We can take the ionization energy of Ar^{39} to be $\approx 23.6keV$, then:

$$1electron = 23.6keV$$

and

$$1electron = 1.602 * 10^{-19} C$$

Then $\frac{dE}{dQ}$ becomes:

$$\frac{dE}{dQ} = \frac{23.6keV}{1.602 * 10^{-19} C} \tag{2.10}$$

Finally, we calculate the result of equation **??** and convert to units of $\frac{GeV}{mm}$.

$$\frac{dE}{dx}_{max} = 1.875 * 10^{-11} \frac{C}{m} * \frac{23.6keV}{1.602 * 10^{-19} C} \approx 2.76 \frac{GeV}{mm} \tag{2.11}$$

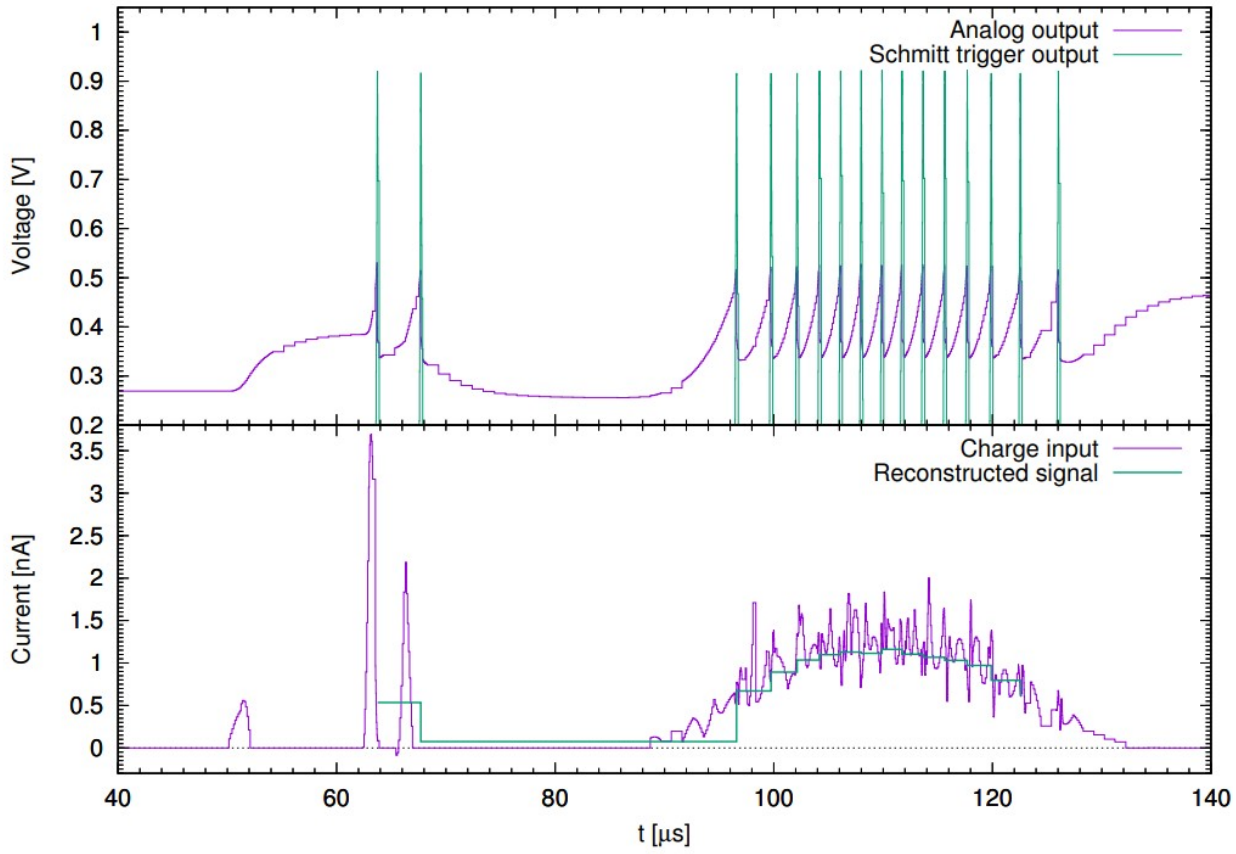

Figure 2.2: Example reconstruction of the reset time difference (RTD) based on the Q-Pix readout design. Image is taken from [74].

Background Calibration

Calibration measurements are essential for any detector. Here we describe an automatic use of existing Ar^{39} decays as a source of calibration at the pixel level.

The value which needs to be calibrated is the pixel's response to an input charge Q_{in} in equation 2.1. Given some stable input charge, there should be a known number of reset measurements to calibrate against.

The capacitance (C_i) for each pixel is a systematic which can be calibrated periodically using the background current from Ar^{39} decay.

Once the trigger voltage (V_i) is exceeded the schmidt trigger issues the timing reset which is then

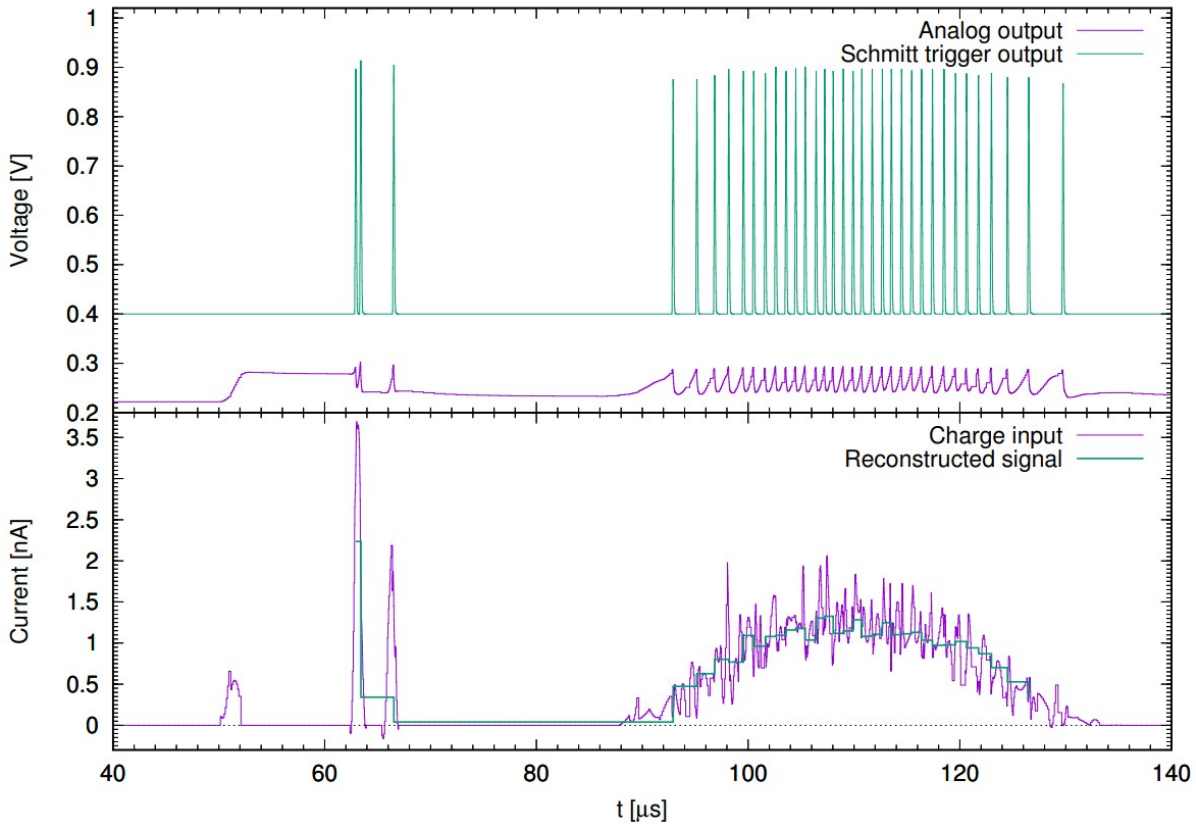

Figure 2.3: Example reconstruction of the reset time difference (RTD) based on the Q-Pix readout design. delta-Q was chosen to be $0.3fC$. Image is taken from [74].

recorded as a 32-bit digital timestamp. This timestamp value is recorded against a free running local oscillator ($\approx$ 30 MHz). The number of free running clocks in the entire system is expected to be the number of channels (N_c) divided by the number of digitally multiplexed channels (N_d), which are taken to be 16.

Making a 3-D Image

One of the important features of a TPC is the ability to reconstruct full 3-D images. The intended benefit of a pixelated readout on any TPC is to show that there are improvements to reconstruction of these 3-D images.

In order to reconstruct the image of the interaction from a set of data above the pixel the required data are the reset time at a pixel i (T_{ri}), event time (T_e), and the pixel ID. We assume that T_e (as is normally used to tag events in TPCs) uses a trigger time from a secondary PMT system from

the scintillation light produced by the interaction to tag an event of interest. Since the scintillation photons travel much faster than the drift electrons, we can use the T_e as the starting time.

The pixel ID of each reset gives two of the three remaining coordinates ($\hat{x}$ and $\hat{y}$). The last coordinate ($\hat{z}$) is reconstructed using T_{ri}.

Since the drift velocity of the electrons (v_e) is constant in a TPC the distance that the electrons traveled to reach the anode plane ($\hat{z}$) is determined based on only the drift time:

$$z = v_e * T_{drift} \tag{2.12}$$

However, this drift time is measured directly from the difference between the event time (T_e) and the reset time for this pixel (T_{ri}).

$$T_{drift} = T_{ri} - T_e \tag{2.13}$$

The drift distance in equation (2.1) becomes:

$$z = v_e * (T_{ri} - T_e) \tag{2.14}$$

Uncertainties

Therefore the precision of the measurement of $\hat{z}$ is based on equation 2.1. The uncertainty for the two transverse coordinates on the anode plane ($\hat{x}$ and $\hat{y}$) which are reasonable assumed to be uniform over the pixel are then $\frac{3mm}{\sqrt{12}} \approx 0.87mm$.

Bad Scenarios

Here we briefly describe potential issues of the readout circuit presented here.

Maximum Reset Rate

2.2 System Requirements

This differs from other concepts such as Genetic Multiplexing ([75]) and using only regions of interest (ROI).

Therefore, the total number of free running oscillators (N_{osc}) per DUNE-APA for a given pixel pixel of 3 mm^2 is:

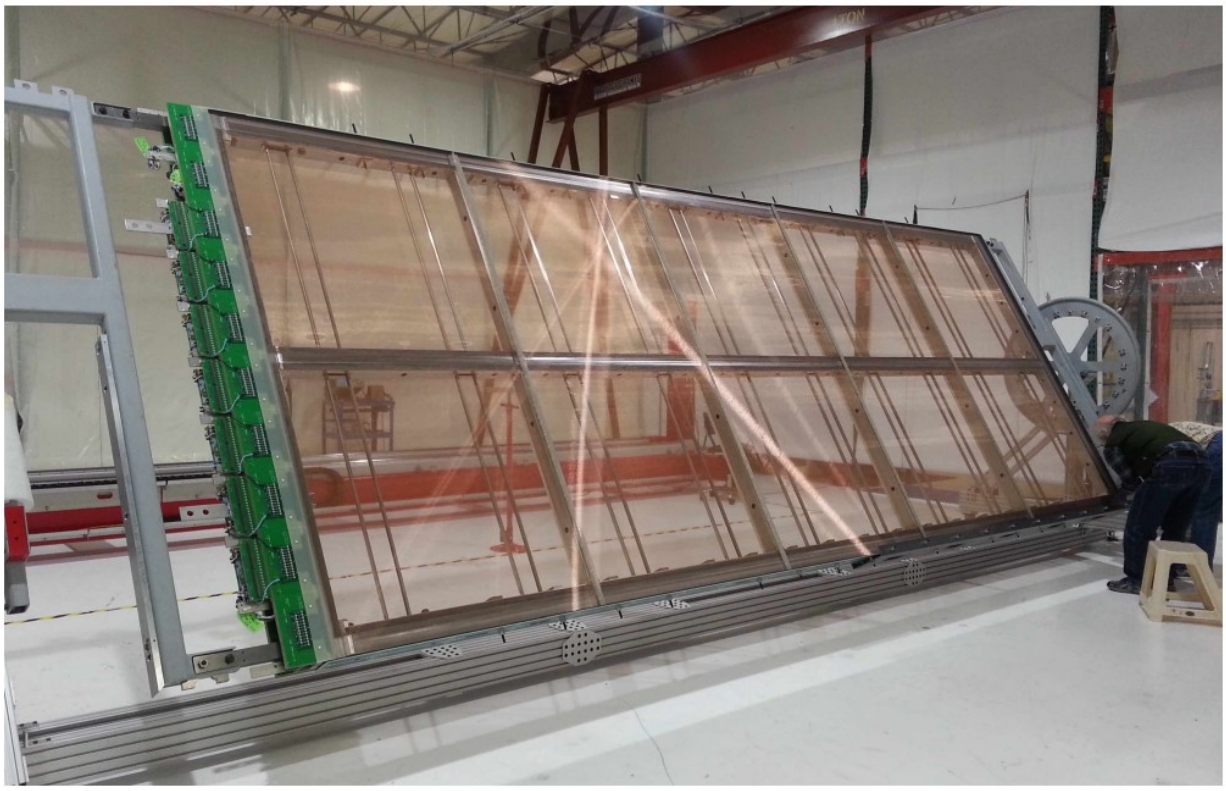

Figure 2.4: A simple caption [70]

$$N_{osc} = \frac{6.3 * 2.5}{9 * 10^{-6} * 16} = 109375 \tag{2.15}$$

Therefore we expect the order of the number of free running oscillators per DUNE-APA $O(10^5)$.

Single Point Failures

2.3 How Q-Pix fits into a DUNE APA

DUNE Anode Plane Assemblies (APA) designs are based on [70].

Chapter 3

NEW DIFFUSION MEASUREMENTS: STUDIES WITHIN SAQ

In this chapter we introduce the first implementation of the Q-Pix based design using purely "over-the-counter" electronics.

3.1 Simplified Analog Q-Pix: System Design

3.2 Leakage Current Measurements

3.3 TPC Design

3.4 Diffusion in Noble Gasses

Measurements of Transverse and Longitudinal diffusion of electrons within electric fields of strength 500 V/cm have been performed before [76].

3.5 Measurements of Drift Current

3.6 LArTPC Diffusion background

3.7 Xenon Gas Lamp Measurements

Integrating towards background Current

3.8 Results

Chapter 4

THE DIGITAL BACK-END AND VIABILITY STUDIES

In this chapter we describe the overall structure digital back-end of the Q-Pix design. We would like to take a moment here to note here that we refer to each node in the array is implemented as a lattice ice40UP FPGA

Additionally, this chapter is divided into two parts. The first part we give a detailed description of the digital-system, and its requirements to successful in a Q-Pix based detector of DUNE scales. The motivation here is to outline how the digital backend of Q-Pix based readout fits into the DUNE-FD LArTPC. The second part of this chapter is dedicated to the first evaluation boards developed and tested which are implemented in Lattice iCE40UP FGPAs [77]. The second part outlines the design of the PCB on which these FPGAs are implemented, as well as basic results of these FGPAs, which are motivated from the first part of this chapter.

The Lattice Semiconductor FPGAs [77] were selected because of the small form factor, pin out, availability, as well as lower power consumption. There are planned tests for future, but not presented here to indicate its viability of over-the-counter FPGAs in LArTPc. If such cheap and available FPGAs were shown to be reliable use in a LArTPC environment, that would greatly influence future detector development and selection for Q-Pix.

4.1 Digital Design Overview

The digital system of the entire Q-Pix design begins at the electronic collection of a recorded timestamp in respond to a reset-time-difference sent from the analog front-end. Then, all data that are recorded for each pixel, and the only data required for a full analysis of all reconstruction with a LArTPC are:

- 32 bit timestamp
- Pixel X location ($\leq$ 4 bits)
- Pixel Y location ($\leq$ 4 bits)
- APA reference number ($\leq$ 4 bits)

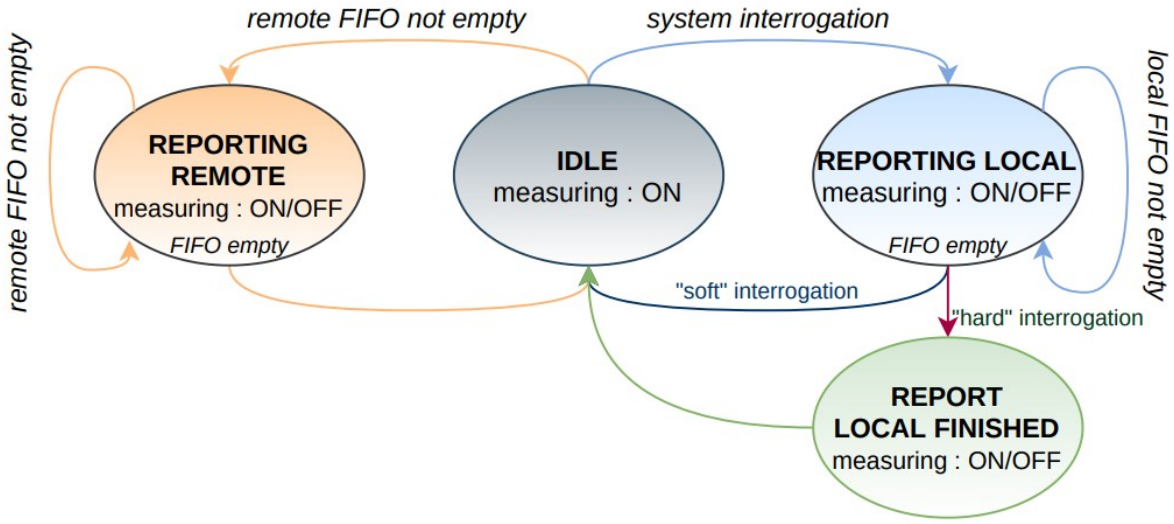

Figure 4.1: Diagram of the Digital node's FSM which determines how to respond to incoming packets.

Each of these remote ASICs are running on free-running independent clocks, with an expected frequency of $\approx$ 30 MHz.

Basic System Requirements

Reset time differences are a function of the accumulated charge compared to the integrating capacitance for this specific pixel. The sheer number of pixels required for an APA (and the entire module) require an effective means of charge and time calibration, stable buffer depths, and protection against single-point failure (SPF).

Charge Calibration of each Pixel

Natural decay products produced by $^{3}9$Ar provide a continous source of incoming current across a LArTPC.

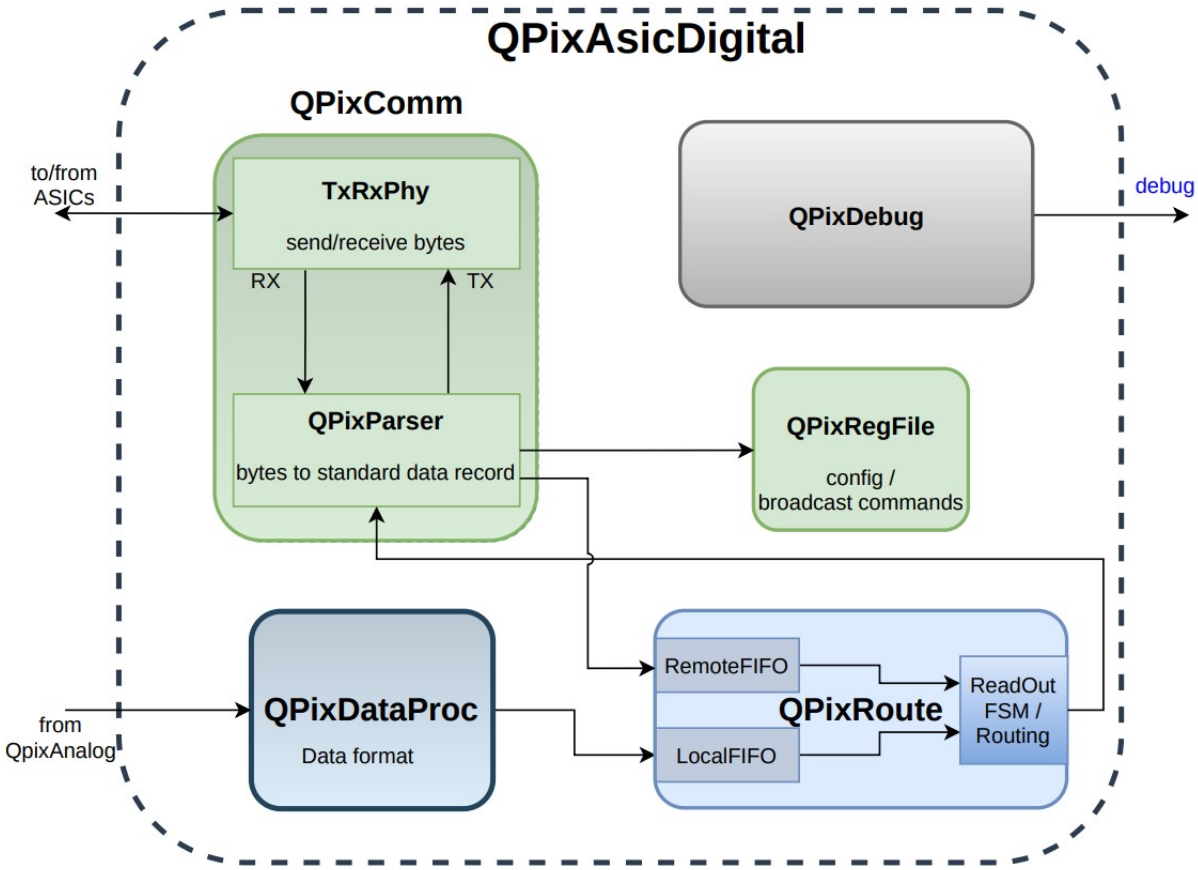

Figure 4.2: Diagram of the Digital node.

Time Calibration of each Node

Inter-Node communication via endeavor protocol

The Structure of a Data Word

Each node communicates via an entire packet, which is always 64 bits long. The communication protocol (4.1)

Comments on Data Rates and required Computing

Based on the minimum number of bits for each RTD 4.1 we can calculate minimum data rates for a full APA section and extend to this to

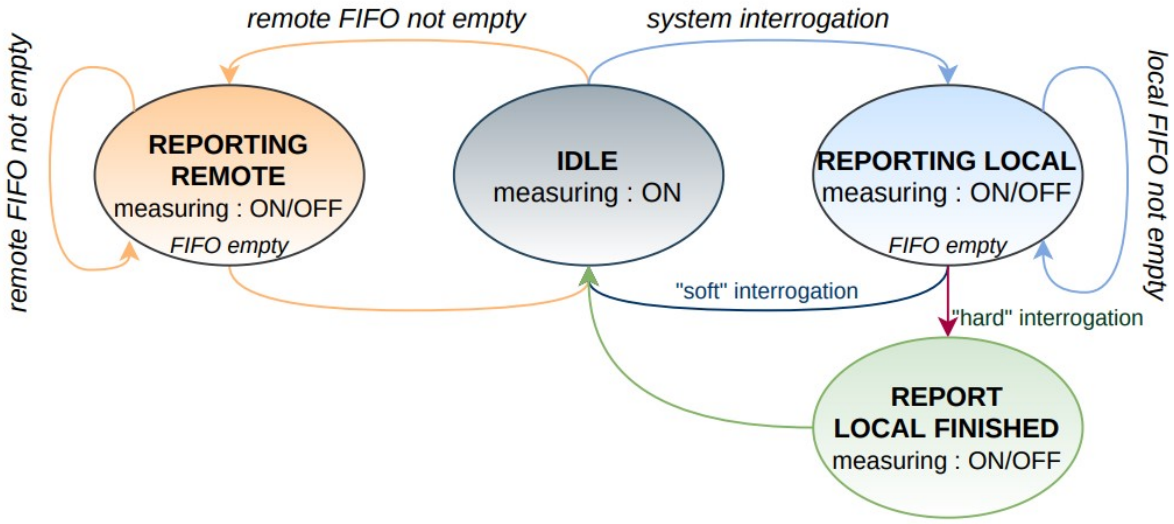

Figure 4.3: Overview of the FSM design, courtesy of Vasily Shebalin.

4.2 The Digital Finite State Machine

The Finite State Machine (FSM) of the remote digital ASIC outlines the designed behavior response to inputs from a controlling DAQ node.

- Idle, Acquisition State
- Transmit Local
- Transmit Finish
- Transmit Remote
- DONE

4.3 The Parameter Space of the Digital System

Buffer Depth Requirements

The required buffer depth of each node in an array is the maximum number of timestamps the node can store in memory before running out of room.

4.4 QDB Design Overview

4.5 Power and Current Characteristics

4.6 Timing Stability

We describe here the methods of measuring a stable time for different configurations of the nodes. We also comment on the results of the timing with resepect to the minimum required timing sensitivity in order to have accurate timestamp reconstruction.

4.7 Analysis of Systematics for Different System Implementations

4.8 Towards the Integration of a DAQ-Node

4.9 Comments on A Super-DAQ-Node

Each APA module within a larger DUNE module must ultimately be interconnected so that the entire module can be readout. As described above, a single modular tile is controlled by an individual DAQ node, where many constitute a complete APA. Therefore, we refer to the device that digitally multiplexes all of the DAQ node data as the "Super DAQ Node" (SDN). Then, we imagine the final multiplexing stage for an entire DUNE module as an array of SDNs, each of which consistute an array of DAQ nodes, where each DAQ node is a 2-D array of Q-Pix based ASICs.

The total number of request SDNs within the full dune module depends on the final size of a DAQ-node controlled tile.

4.10 Summary

Chapter 5

SIMULATION STUDIES AND FUTURE Q-PIX PROTOTYPES

5.1 Physical Simulation Studies

5.2 Background Rates and Calibration

sources of backgrounds are taken from [70]

5.3 Supernova Studies

Work has been done to understand how a Q-Pix based DUNE-FD would measure core collapse supernovae [78].

Simulation studies which involved particle interactions were based on Geant4 [79].

5.4 Looking for Hadron Decay

5.5 Neutrino Beam High Energy Studies

5.6 Further Studies

Chapter 6

SUMMARY AND OUTLOOK

Recap of Qpix Requirements for DUNE APA here.

Recap of Qpix design concept testing within SAQ here.

Recap of QDB Results here

Recap of SAQ Results here

Recap of lessons learned on pixelated detectors

Discuss how combination of simulation / qdb / saq results motivate the next stage of development for QPix and incorporating the digital / analog ASICs for round two.

BIBLIOGRAPHY

[1]S. L. Glashow, "Partial-symmetries of weak interactions", Nuclear Physics **22**, 579–588 (1961).

[2]A. Salam and J. C. Ward, *Electromagnetic and weak interactions*, tech. rep. (IMPERIAL COLL OF SCIENCE and TECHNOLOGY LONDON (ENGLAND), 1964).

[3]S. Weinberg, "A model of leptons", Physical review letters **19**, 1264 (1967).

[4]R. L. Workman and Others, "Review of Particle Physics", PTEP **2022**, 083C01 (2022).

[5]D. Dominguez, *Cern accelerating science*, 2015.

[6]M. Gell-Mann, "The Eightfold Way: A Theory of strong interaction symmetry", 10.2172/4008239 (1961).

[7]M. Gell-Mann, "A schematic model of baryons and mesons", Physics Letters **8**, 214–215 (1964).

[8]J. J. Aubert, U. Becker, P. J. Biggs, J. Burger, M. Chen, G. Everhart, P. Goldhagen, J. Leong, T. McCorriston, T. G. Rhoades, M. Rohde, S. C. C. Ting, S. L. Wu, and Y. Y. Lee, "Experimental observation of a heavy particle J", Phys. Rev. Lett. **33**, 1404–1406 (1974).

[9]E. D. Bloom, D. H. Coward, H. Destaebler, J. Drees, G. Miller, L. W. Mo, R. E. Taylor, M. Breidenbach, J. I. Friedman, G. C. Hartmann, and H. W. Kendall, "High-Energy Inelastic e-p Scattering at 6° and 10°", prl **23**, 930–934 (1969).

[10]M. Breidenbach, J. I. Friedman, H. W. Kendall, E. D. Bloom, D. H. Coward, H. Destaebler, J. Drees, L. W. Mo, and R. E. Taylor, "Observed Behavior of Highly Inelastic Electron-Proton Scattering", prl **23**, 935–939 (1969).

[11]S. W. Herb et al., "Observation of a dimuon resonance at 9.5 gev in 400-gev proton-nucleus collisions", Phys. Rev. Lett. **39**, 252–255 (1977).

[12]S. Abachi et al., "Observation of the top quark", Physical Review Letters **74**, 2632–2637 (1995).

[13]S. H. Neddermeyer and C. D. Anderson, "Note on the nature of cosmic-ray particles", Phys. Rev. **51**, 884–886 (1937).

[14]M. L. Perl et al., "Evidence for anomalous lepton production in $e^+ - e^-$ annihilation", Phys. Rev. Lett. **35**, 1489–1492 (1975).

[15]K. Kodama et al., "Observation of tau neutrino interactions", Physics Letters B **504**, 218–224 (2001).

[16]R. Brandelik et al., "Evidence for planar events in e+e- annihilation at high energies", Physics Letters B **86**, 243–249 (1979).

[17]D. P. Barber et al., "Discovery of three jet events and a test of quantum chromodynamics at petra", Phys. Rev. Lett. **43**, 830–833 (1979).

[18]G. Arnison et al., "Experimental observation of isolated large transverse energy electrons with associated missing energy at s=540 gev", Physics Letters B **122**, 103–116 (1983).

[19]G. Arnison et al., "Experimental observation of lepton pairs of invariant mass around 95 gev/c2 at the cern sps collider", Physics Letters B **126**, 398–410 (1983).

[20]P. Higgs, "Broken symmetries, massless particles and gauge fields", Physics Letters **12**, 132–133 (1964).

[21]G. Aad et al., "Observation of a new particle in the search for the standard model higgs boson with the atlas detector at the lhc", Physics Letters B **716**, 1–29 (2012).

[22]J. L. Hewett et al., *Fundamental physics at the intensity frontier*, 2012.

[23]A. Airapetian et al., "ATLAS: Detector and physics performance technical design report. Volume 2", (1999).

[24]G. L. Bayatian et al., "CMS Physics: Technical Design Report Volume 1: Detector Performance and Software", (2006).

[25]T. Abe et al., *Belle ii technical design report*, 2010.

[26]"Juno physics and detector", Progress in Particle and Nuclear Physics **123**, 103927 (2022).

[27]D. A. Glaser, "Some effects of ionizing radiation on the formation of bubbles in liquids", Phys. Rev. **87**, 665–665 (1952).

[28]G. Charpak, R. Bouclier, T. Bressani, J. Favier, and C. Zupancic, "The Use of Multiwire Proportional Counters to Select and Localize Charged Particles", Nucl. Instrum. Meth. **62**, 262–268 (1968).

[29]J. N. Marx and D. R. Nygren, "The time projection chamber", Physics Today **31**, 46–53 (1978).

[30]E. Aprile et al., "The XENON1t dark matter experiment", The European Physical Journal C **77**, 10.1140/epjc/s10052-017-5326-3 (2017).

[31]B. Abi et al., "Volume i. introduction to dune", Journal of Instrumentation **15**, T08008 (2020).

[32]C. Rubbia, *The liquid-argon time projection chamber: a new concept for neutrino detectors*, tech. rep. (1977).

[33]R. Acciarri et al., "Demonstration of mev-scale physics in liquid argon time projection chambers using argoneut", Phys. Rev. D **99**, 012002 (2019).

[34]R. Acciarri et al., "Design and construction of the microboone detector", Journal of Instrumentation **12**, P02017 (2017).

[35]R. Acciarri et al., "The liquid argon in a testbeam (lariat) experiment", Journal of Instrumentation **15**, P04026 (2020).

[36]A. Friedland and S. W. Li, "Understanding the energy resolution of liquid argon neutrino detectors", Phys. Rev. D **99**, 036009 (2019).

[37]F. Arneodo, *The icarus experiment, a second-generation proton decay experiment and neutrino observatory at the gran sasso laboratory*, 2001.

[38]K. Abe et al., "Search for proton decay via $p \to e^+\pi^0$ and $p \to \mu^+\pi^0$ in 0.31 megaton $\cdot$ years exposure of the super-kamiokande water cherenkov detector", Phys. Rev. D **95**, 012004 (2017).

[39]P. Nath and R. Arnowitt, "Limits on photino and squark masses from proton lifetime in supergravity models", Phys. Rev. D **38**, 1479–1484 (1988).

[40]H.-K. Proto-Collaboration et al., *Hyper-kamiokande design report*, 2018.

[41]G. M. Fuller, R. W. Mayle, J. R. Wilson, and D. N. Schramm, "Resonant Neutrino Oscillations and Stellar Collapse", apj **322**, 795 (1987).

[42]J. Chadwick, "The intensity distribution in the magnetic spectrum of beta particles from radium (B + C)", Verh. Phys. Gesell. **16**, 383–391 (1914).

[43]J. S. Chadwick, "Possible existence of a neutron", Nature **129**, 312–312 (1932).

[44]E. Fermi, "Versuch einer Theorie der β-Strahlen. I", Zeitschrift fur Physik **88**, 161–177 (1934).

[45]C. L. Cowan, F. Reines, F. B. Harrison, H. W. Kruse, and A. D. McGuire, "Detection of the free neutrino: a confirmation", Science **124**, 103–104 (1956).

[46]G. Danby, J.-M. Gaillard, K. Goulianos, L. M. Lederman, N. Mistry, M. Schwartz, and J. Steinberger, "Observation of high-energy neutrino reactions and the existence of two kinds of neutrinos", Phys. Rev. Lett. **9**, 36–44 (1962).

[47]F. P. An et al., "Observation of electron-antineutrino disappearance at daya bay", Phys. Rev. Lett. **108**, 171803 (2012).

[48]Q. R. Ahmad et al., "Direct evidence for neutrino flavor transformation from neutral-current interactions in the sudbury neutrino observatory", Phys. Rev. Lett. **89**, 011301 (2002).

[49]M. A. Acero et al., "First measurement of neutrino oscillation parameters using neutrinos and antineutrinos by nova", Phys. Rev. Lett. **123**, 151803 (2019).

[50]K. Abe et al., "Indication of electron neutrino appearance from an accelerator-produced off-axis muon neutrino beam", Phys. Rev. Lett. **107**, 041801 (2011).

[51]J. K. Ahn et al., "Observation of reactor electron antineutrinos disappearance in the reno experiment", Phys. Rev. Lett. **108**, 191802 (2012).

[52]S. Fukuda et al., "Determination of solar neutrino oscillation parameters using 1496 days of super-kamiokande-i data", Physics Letters B **539**, 179–187 (2002).

[53]K. Eguchi et al., "First results from kamland: evidence for reactor antineutrino disappearance", Phys. Rev. Lett. **90**, 021802 (2003).

[54]Y. Abe et al., "Indication of reactor $\overline{\nu}_e$ disappearance in the double chooz experiment", Phys. Rev. Lett. **108**, 131801 (2012).

[55]R. Davis, D. S. Harmer, and K. C. Hoffman, "Search for neutrinos from the sun", Phys. Rev. Lett. **20**, 1205–1209 (1968).

[56]K. Abe et al., "Measurements of neutrino oscillation in appearance and disappearance channels by the t2k experiment with 6.6×10^{20} protons on target", Phys. Rev. D **91**, 072010 (2015).

[57]B. Pontecorvo, "Inverse beta processes and nonconservation of lepton charge", Zh. Eksp. Teor. Fiz. **34**, 247 (1957).

[58]Z. Maki, M. Nakagawa, and S. Sakata, "Remarks on the Unified Model of Elementary Particles", Progress of Theoretical Physics **28**, 870–880 (1962).

[59]X. Qian and P. Vogel, "Neutrino mass hierarchy", Progress in Particle and Nuclear Physics **83**, 1–30 (2015).

[60]L. Wolfenstein, "Neutrino oscillations in matter", Phys. Rev. D **17**, 2369–2374 (1978).

[61]A. Y. Smirnov, "The msw effect and matter effects in neutrino oscillations", Physica Scripta **2005**, 57–64 (2004).

[62]I. Esteban, M. C. Gonzalez-Garcia, M. Maltoni, T. Schwetz, and A. Zhou, "The fate of hints: updated global analysis of three-flavor neutrino oscillations", Journal of High Energy Physics **2020**, 178, 178 (2020).

[63]P Sadowski, B Radics, Ananya, Y Yamazaki, and P Baldi, "Efficient antihydrogen detection in antimatter physics by deep learning", Journal of Physics Communications **1**, 025001 (2017).

[64]P. Sadowski and P. Baldi, "Deep learning in the natural sciences: applications to physics", in Braverman readings in machine learning (2017).

[65]D. Dwyer, M. Garcia-Sciveres, D. Gnani, C. Grace, S. Kohn, M. Kramer, A. Krieger, C. Lin, K. Luk, P. Madigan, C. Marshall, H. Steiner, and T. Stezelberger, "Larpix: demonstration of low-power 3d pixelated charge readout for liquid argon time projection chambers", Journal of Instrumentation **13**, P10007 (2018).

[66]J. Asaadi, M. Auger, A. Ereditato, D. Goeldi, R. Hänni, U. Kose, I. Kreslo, D. Lorca, M. Luethi, C. R. von Rohr, J. Sinclair, F. Stocker, C. Tognina, and M. Weber, "A pixelated charge readout for liquid argon time projection chambers", Journal of Instrumentation **13**, C02008 (2018).

[67]F. Sutanto, T. Classen, S. Dazeley, M. Duvall, I. Jovanovic, V. Li, A. Mabe, E. Reedy, and T. Wu, "Sandd: a directional antineutrino detector with segmented 6li-doped pulse-shape-sensitive plastic scintillator", Nuclear Instruments and Methods in Physics Research Section A: Accelerators, Spectrometers, Detectors and Associated Equipment **1006**, 165409 (2021).

[68]B. Abi et al., *Deep underground neutrino experiment (dune), far detector technical design report, volume ii: dune physics*, 2020.

[69]B. Abi et al., "Volume iii. dune far detector technical coordination", Journal of Instrumentation **15**, T08009 (2020).

[70]B. Abi et al., "Volume iv. the dune far detector single-phase technology", Journal of Instrumentation **15**, T08010 (2020).

[71]R. Acciarri et al., *Long-baseline neutrino facility (lbnf) and deep underground neutrino experiment (dune) conceptual design report volume 1: the lbnf and dune projects*, 2016.

[72]L. Paulucci and on behalf of DUNE collaboration, "The dune vertical drift photon detection system", Journal of Instrumentation **17**, C01067 (2022).

[73]J. Joshi and X. Qian, *Signal processing in the microboone lartpc*, 2015.

[74]D. Nygren and Y. Mei, *Q-pix: pixel-scale signal capture for kiloton liquid argon tpc detectors: time-to-charge waveform capture, local clocks, dynamic networks*, 2018.

[75]S. Procureur, R. Dupré, and S. Aune, "Genetic multiplexing and first results with a 50×50cm2 micromegas", Nuclear Instruments and Methods in Physics Research Section A: Accelerators, Spectrometers, Detectors and Associated Equipment **729**, 888–894 (2013).

[76]Y. Li, T. Tsang, C. Thorn, X. Qian, M. Diwan, J. Joshi, S. Kettell, W. Morse, T. Rao, J. Stewart, W. Tang, and B. Viren, "Measurement of longitudinal electron diffusion in liquid argon", Nuclear Instruments and Methods in Physics Research Section A: Accelerators, Spectrometers, Detectors and Associated Equipment **816**, 160–170 (2016).

[77]Lattice, *Ice40 ultraplus family data sheet*, lattice ice40up fpga data sheet, Lattice Semiconductor (https://www.latticesemi.com/-/media/LatticeSemi/Documents/DataSheets/iCE/iCE40-UltraPlus-Family-Data-Sheet.ashx).

[78]S. Kubota et al., "Enhanced low-energy supernova burst detection in large liquid argon time projection chambers enabled by q-pix", Phys. Rev. D **106**, 032011 (2022).

[79]S. Agostinelli et al., "Geant4—a simulation toolkit", Nuclear Instruments and Methods in Physics Research Section A: Accelerators, Spectrometers, Detectors and Associated Equipment **506**, 250–303 (2003).

[80]A. Galindo-Tellez, K. Keefe, E. Adamek, E. Brubaker, B. Crow, R. Dorrill, A. Druetzler, C. J. Felix, N. Kaneshige, J. G. Learned, J. J. Manfredi, K. Nishimura, B. Pinto Souza, D. Schoen, and M. Sweany, "Design and calibration of an optically segmented single volume scatter camera for neutron imaging", Journal of Instrumentation **16**, P04013, P04013 (2021).

Appendix A

SVSC OS1

the work in this subsection details the work and results of [80].

Appendix B

SVSC OS2

Put OS2 work here